Alpha and beta radiation effects on Re_2MnCoO_6 (Re = La, Sm, Nd)

Tinashe Dhliwayo[1,2], Odireleng M Ntwaeaborwa[3] and Buyisiwe M Sondezi[1]

[1]Rare Earth-Based Oxides and Nano Group, Department of Physics, University of Johannesburg, Cnr Kingsway Avenue and University Road, Auckland Park 2006, South Africa.
[2]Advanced Energy, Abu Dhabi Polytechnic, MBZ, Abu Dhabi, UAE.
[3] Department of Physical and Earth Sciences Sol-Plaatjie University, Kimberly, South Africa.

E-mail: Tinashe.dhliwayo@actvet.gov.ae

Abstract. The rise in global demand for nuclear technology has led to an increase in radioactive waste and radioactive materials. Some of these radioactive materials and nuclear waste undergo radioactive decay, emitting alpha and beta particles. Both alpha and beta particles can cause significant damage along their path of travel. Consequently, there is a need to identify/develop materials suitable for use in radiation shielding. This study, therefore, aimed at investigating the effects of alpha and beta radiation on Re_2MnCoO_6 (Re = La, Sm, Nd) prepared by the solid-state method. The continuous slowing-down approximation (CSDA) range of beta particles in the samples and the stopping power of the samples have been calculated using the ESTAR method. At 0.5 MeV, the CSDA range of beta particles is 0.273 g/cm^2 for Sm_2MnCoO_6, 0.270 g/cm^2 for Nd_2MnCoO_6, and 0.269 g/cm^2 for La_2MnCoO_6. The mass stopping power of all three samples decreases with energy up to 1 MeV, beyond which it starts to increase again. The ion ranges, energy deposition, and displacement damage caused by alpha particles have been estimated using the ion transport Monte Carlo simulations using the Stopping and Range of Ions in Matter (SRIM) code with the Full Damage Cascades Mode. A 4 MeV alpha particle has a range of about 23.3 µm in Sm_2MnCoO_6, 22.7 µm in Nd_2MnCoO_6, and 22.3 µm in La_2MnCoO_6. The mass stopping power for all three samples ranged between 0.320 MeV.cm^2/g and 0.414 MeV.cm^2/g for a 0.1 MeV alpha particle. The results show that double perovskites are possible candidates as matrices for radioactive waste immobilization.

1 Introduction and Background

The rise in global demand for energy has generated interest in the use of nuclear energy across the globe and especially in Africa and the Middle East. This, therefore, means large amounts of spent nuclear fuel and other nuclear-related waste will be produced.

Nuclear waste can be classified as high-level waste (HLW), intermediate-level waste (ILW), and low-level waste (LLW) based on its radioactivity level. Even though HLW has the lowest volume [1, 2] but it is considered the most hazardous because it is highly radioactive, generates large amounts of heat, and contains long-lived radionuclides [3]. The main sources of radiation in nuclear waste are beta decay from fission products and alpha decay of the actinide elements [3]. The recoil nuclei and gamma rays also contribute to the radiation damage of the material. Polonium-212 ($E_\alpha \approx 8.78\ MeV$) and polonium-213 ($E_\alpha \approx 8.38\ MeV$) are some of the actinides with the most energetic alpha emissions. Fission products like yttrium-90 ($E_\beta \approx 2.28\ MeV$) and rhodium-106 ($E_\beta \approx 3.54\ MeV$) are amongst the highest beta emitters.

Disposal of waste depends on the category of the radioactive waste and ranges from landfill to deep geological repositories [4]. High-level waste is proposed to be disposed of using a multi-barrier system,

of which the first barrier is the wasteform [5]. High-level waste needs to be immobilized into a suitable waste form before it can be stored in a multi-barrier system. Immobilization is a process where the waste is made immovable in the form of wasteforms [6]. There are different ways of making wasteforms, such as vitrification, solidification, and containment [7], and the effectiveness of the wasteform is determined by the chemical durability and radiation durability of the matrix. The wasteforms can be classified into three main types, namely glass, ceramic, and glass–ceramic wasteforms.

This study investigates the effects of alpha and beta radiation on selected double perovskite ceramics, possible candidates for ceramic wasteform. Double perovskites are represented by a general formula $A_2BB'O_6$, where A is a lanthanide cation, B and B′ are transition cations. These materials are of interest because of their structural and compositional flexibility [8].

2 Materials and Methods

2.1 Synthesis of materials

Samples were synthesized using the solid-state method [9]. The stoichiometric ratios of the starting powder materials were measured and ground into fine powders and were calcined at 900 °C for 12 hours before being annealed at 1200 °C further for 48 hours. The annealed samples were finely ground and were characterized by powder X-ray diffraction (XRD) to ascertain that the right structures were crystallized. These were achieved through continuous scanning using Cu-Kα radiation (40 kV, 30 mA) at the range between 10° and 90° with a step of 0.02° and a speed of 0.145 s/step.

2.2 Radiation damage measurements

The continuous slowing-down approximation (CSDA) range of beta particles in the samples and the stopping power of the samples were calculated using the ESTAR software. ESTAR is a radiation simulation software developed by the National Institute of Standards and Technology (NIST) to calculate the stopping powers and ranges of electrons as they pass through various materials. The ranges, energy deposition, and displacement damage caused by alpha particles were calculated by the ion transport Monte Carlo simulations using the Stopping and Range of Ions in Matter (SRIM) code with the Full Damage Cascades mode. The energy range of the alpha particles varied from 0 MeV to 10 MeV and from 0 MeV to 4 MeV for beta particles.

3 Results

3.1 XRD and Rietveld analysis

Figures 1a, 1b, and 1c represent powder X-ray diffraction curves of La_2MnCoO_6 (LMCO), Sm_2MnCoO_6 (SMCO), and Nd_2MnCoO_6 (NMCO), respectively. All reflections were indexed according to the Bragg law, and all samples were indexed to a monoclinic structure [9]. Table 1 shows the refinement parameters of the three samples, and these values are consistent with the data published in the literature [10-12]. The volume of the oxides decreases with the increase in the lanthanide ion radius. However, the density increases as the volume decreases due to the increase in mass of the lanthanide ion.

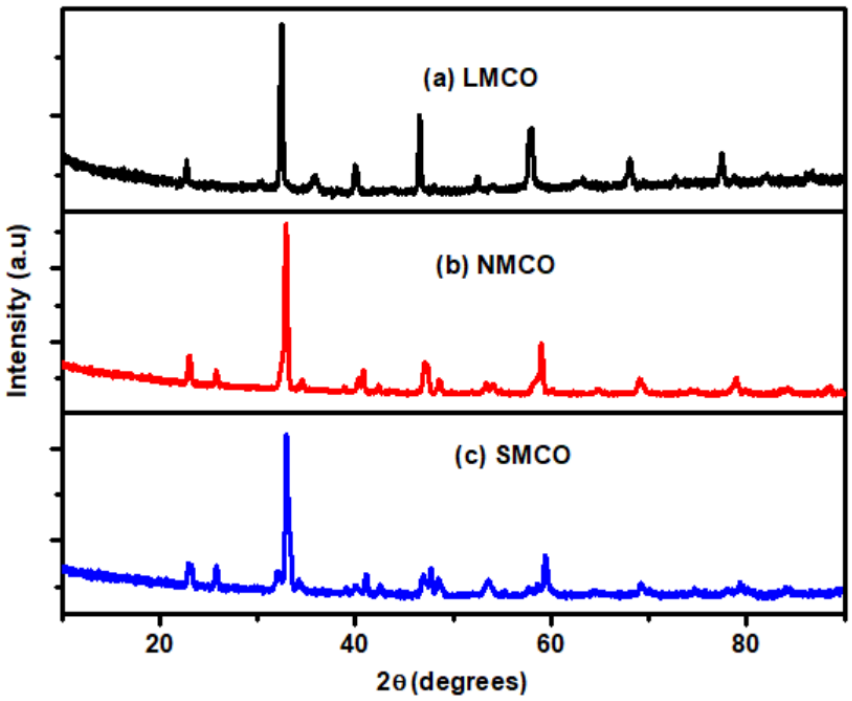

Figure 1: XRD data for LMCO, NMCO, and SMCO

Cell parameters	LMCO	NMCO	SMCO
a (Å)	5.525	5.447	5.360
b (Å)	5.486	5.619	5.564
c (Å)	7.774	7.713	7.607
β (°)	89.880	89.443	90.004
V ($Å^3$)	235.6	228.3	226.9
ρ (gcm^{-3})	3.437	3.512	3.598

Table 1: Sample parameters after refinement.

3.2 Stopping power

Stopping power is the average energy lost by ionizing radiation per unit distance travelled in a medium. The energy is lost through ionization, excitation, and Bremsstrahlung radiation. It is affected by the type of charged particle, energy of the charged particle, and material density and atomic number of the material. The Bethe formula shown in equation 1 is used to calculate the stopping power of materials.

$$-\frac{dE}{dx} = 4\pi \frac{z^2 e^4}{m_e v^2} NB \quad (1)$$

where m_e is the electron mass, v is the particle speed, N is the atomic density of the medium, and B is a variable that is proportional to the atomic number of the medium, Z. The ratio of stopping power and density of the material gives the specific energy loss (mass stopping power). Figures 2a and 2b show the

variation of mass stopping power of different materials with alpha particle energy and beta particle energy, respectively. All three samples show that the alpha particle starts picking up electrons at the energy (E_{max}) of between 0.65 MeV and 0.8 MeV, and the slowing down process starts as shown in Figure 2a. LMCO has the highest stopping power across the energy range under investigation, compared to the other two samples, as illustrated in Figure 2a. This shows that LMCO is more effective in stopping alpha particles with the energy of between 0.01 MeV and 10 MeV.

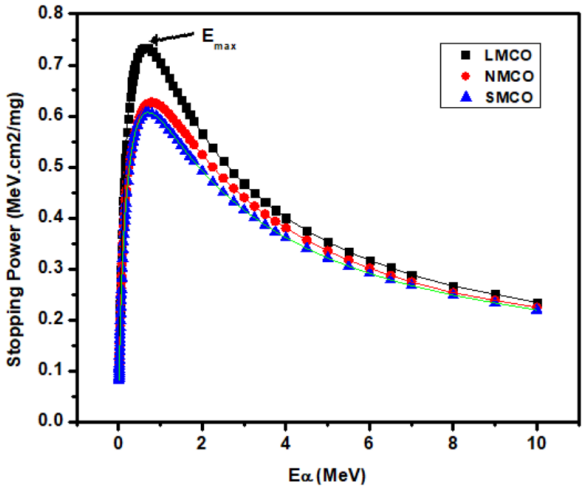

Figure 2a. Specific energy loss as a function of alpha particle energy

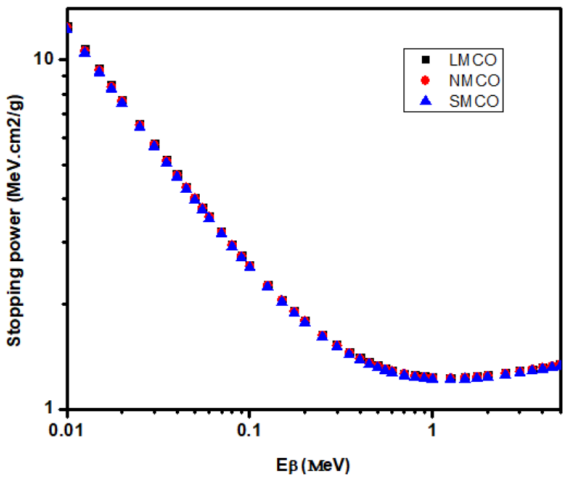

Figure 2b. Specific energy loss as a function of beta particle energy.

However, the stopping power of the materials decreases with beta energy up to about 1.250 MeV and then slowly increases, as shown in Figure 2b. This is because at high energies the beta particle starts behaving like a relativistic particle, and the Bethe formula is no longer applicable. All three materials have similar stopping powers across the energy range under investigation.

3.3 The range and CSDA range

Range is the average depth of penetration of a particle in a material before losing all its energy. The Continuous Slowing Down Approximation (CSDA) concept assumes that the particle loses energy continuously and gradually, without any abrupt changes due to scattering or other interactions. It is calculated using equation 2:

$$R_{CSDA} = \int_0^{E_0} \frac{1}{S(E)} dE \qquad (2)$$

where *S(E)* is the stopping power and E_0 is the incident energy of the radiation particle.

Figure 3a shows the variation of range (μm) as a function of alpha particle energy. The range of alpha particles in all the materials increases with the alpha particle energy. Apha particles have a shorter range in LMCO compared to the other two samples. Again, this shows that LMCO stops alpha particles faster compared to the other two materials. Figure 3b shows that the CSDA ranges for beta particles increase with the energy of the particles, and the ranges are the same in all three samples.

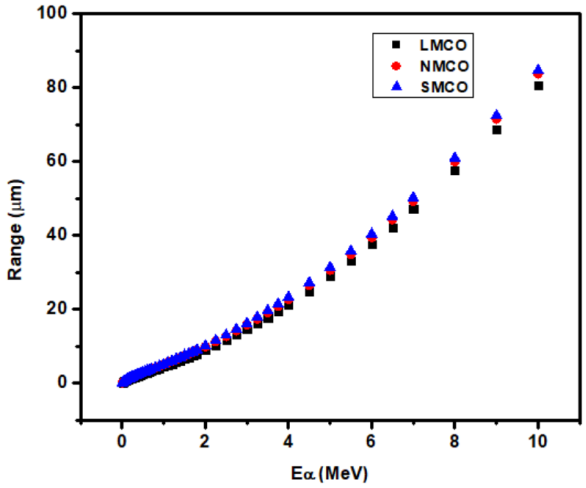

Figure 3a. Variation of range as a function of alpha particle energy.

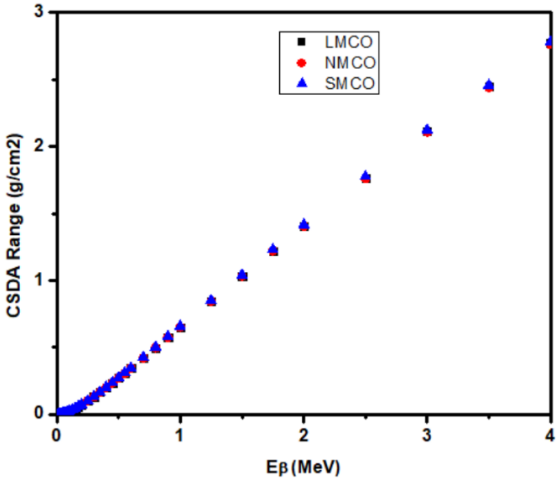

Figure 3b. Variation of range as a function of beta particle energy.

3.4 Alpha particle collision events

SRIM uses the Norgett-Robinson-Torrens (NRT) model, shown in equation 3, to calculate the number of vacancies created and displacements caused [13].

$$\nu_{NRT} = \frac{\kappa T_d}{2E_d} \tag{3}$$

where κ (~0.8) is the displacement efficiency, T_d (MeV)is the average damage energy, and E_d (MeV) is the displacement energy. The model defines a vacancy as the number of times an atom is displaced from its lattice position [13]. Figures 4a, b, and c illustrate the full cascade collision events of the alpha particles in the three materials. A single 8.78 MeV alpha particle created 206 vacancies, 208 vacancies, and 286 vacancies for LMCO, NMCO, and SMCO, respectively. This shows that there is little damage caused by the alpha particle in LMCO compared to the other two materials. The displacement density of the collision cascade increases with an increase in atomic density of the material.

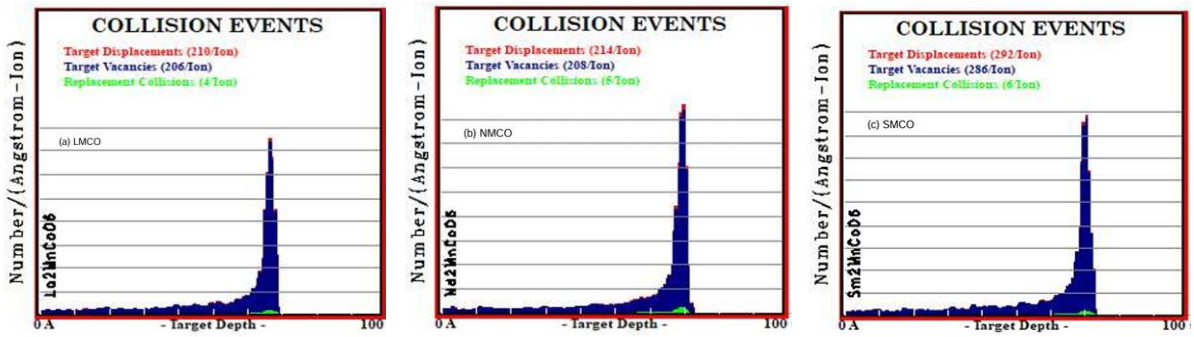

Figure 4 Collision events of an 8.78 MeV alpha particle in LMCO, NMCO, and SMCO

4 Conclusion

We synthesized LMCO, NMCO, and SMCO using the solid-state reaction method. All samples were indexed to a monoclinic structure that belongs to a space group $P2_1/n$ (14) using XRD analysis. The mass stopping power and particle ranges were measured using SRIM for alpha particles and ESTAR for beta particles. LMCO performed better than the other two materials when irradiated with alpha particles, but all three performed the same when irradiated with beta particles. For a 1 MeV beta particle, the stopping powers of the materials are 1.234 MeV/(g/cm^2), 1.231 MeV/(g/cm^2), and 1.217 MeV/(g/cm^2) for LMCO, NMCO, and SMCO, respectively. An 8 MeV alpha particle has a range of 57.6 μm in LMCO, 60.0 μm in NMCO, and 61.0 μm in SMCO. The analysis of the obtained results suggests that double perovskites are radiation tolerant, but further analysis needs to be done on the chemical durability, loading capacity, and durability under aqueous conditions.

5 References

[1] J. S. McCloy, A.G., *Glass-ceramics for nuclear-waste immobilization.* MRS Bulletin, 2017. 42.

[2] R. K. Pilania, L.C.D., *Matrices for radioactive waste immobilization: a review.* Frontiers in Materials, 2023. 10.

[3] D. J. Gregg, J.S.M., J. D. Vienna, A. M. Macfarlane, W. J. Weber, G. R. Lumpkin, *Glass and ceramic nuclear waste forms: The scientific battle.* Bulletin of the Atomic Scientists, 2025. 81.

[4] S. A. Darda, H.A.G., V. Damideh, M. Aboughaly, I. Hassen, *A comprehensive review on radioactive waste cycle from generation to disposal.* Radioanal. Nucl. Chem, 2021. 329.

[5] C. M. Jantzen, M.I.O., *On selection of matrix (wasteform) material for higher activity nuclear waste immobilization (review).* Russ. J. Inorg. Chem, 2019. 64.

[6] Y. Jo, K.G., N. Çevirim-Papaioannou, O. D. Blanco, B. de Blochouse, M. Altmaier, et al., *Solubility of niobium(V) in cementitious systems relevant for nuclear waste disposal: characterization of the solubility-controlling solid phases.* J. Hazard. Mater, 2022. 440.

[7] J. Li, D.X., X. Wang, K. Liu, Y. Mao, M. Wang, et al, *Encapsulation of cesium with a solid waste-derived sulfoaluminate matrix: A circular economy approach of treating nuclear wastes with solid wastes.* J. Hazard. Mater, 2021. 146.

[8] K. Ji, Y.Y., G.T. Moyo, C. Ritter, J. P. Attfield, *Double and double double perovskites in the $RMnMnTaO_6$ series.* Journal of Solid State Chemistry, 2022. 313.

[9] R.C. Sahoo, S.D., T.K. Nath, *Effect of rare earth site substitution on magnetic and transport properties of Ln_2CoMnO_6 (Ln = La, Sm and Gd) double perovskites.* Journal of Magnetism and Magnetic Materials, 2018. 460: p. 409–417.

[10] K. Yi, Q.T., Z. Wu, X. Zhu, *Unraveling the Structural, Dielectric, Magnetic, and Optical Characteristics of Nanostructured La_2NiMnO_6 Double Perovskites.* Nanomaterials, 2022. 12.

[11] F. Aafreen, S.M., G. Saurabh *Functional properties of A-site cation ordered phases derived from La2MnNiO6 double perovskites.* Physica B: Condensed Matter, 2023. 655.

[12] S. Lei, Z.X.-Q., D. Qiao-Yan, K. Ya-Jiao, H. Kai-Yue, L. Cheng-Shi, C. Zhao-Hua, *Magnetocaloric effect and critical behaviors of R_2NiMnO_6 (R =Eu and Dy) double perovskite oxides.* Journal of Alloys and Compounds, 2018. 746.

[13] S. Agarwal, Y.L., C. Li, R.E. Stoller, S.J. Zinkle, *On the use of SRIM for calculating vacancy production: Quick calculation and full-cascade options.* Beam Interactions with Materials and Atoms, 2021. 503.